Polar interval-based localization in mobile sensor networks

Farah Mourad-Chehade, Paul Honeine, Hichem Snoussi

Polar interval-based localization in mobile sensor networks

Farah Mourad, Paul Honeine, and Hichem Snoussi

***Abstract*—This paper considers the problem of localization in uncontrolled mobility sensor networks. Based on connectivity measurements, the problem is solved using polar intervals. Computation is performed, in several polar coordinate systems, using both polar coordinates and interval analysis. Position estimates are thus partial rings enclosing the exact solution of the problem. Simulation results corroborate the efficiency of the proposed method compared to existing methods, especially to those handling single coordinate systems.**

***Index Terms*—mobile sensor networks, multi-coordinate systems, polar intervals, state estimation.**

I. Introduction

MOBILE Sensor Networks (MSN) are networks composed of a large number of wireless devices having sensing, computing and communication capabilities [1], [2]. Due to their wireless aspect, sensors in MSN are able to move, either in a controllable or in an uncontrollable manner. In the first case, sensors are robots having locomotion capabilities as well [3], [4]. One could here manage the mobility of the robots to improve the accuracy of the collected data [5], [6]. In the second case, sensors move in a passive manner, due to external forces, and thus they need to be localized regularly [7], [8]. Many applications have been considered for MSN in military, such as target tracking and enemy surveillance, and in civil domains, such as environment monitoring, healthcare and so on [9], [10]. In all applications, it is of great importance to have correct sensors positions, since sensed data are tightly related to the locations where measurements are made.

Many works have considered the problem of localization in uncontrolled mobility sensor networks [11], [12]. The first intuitive solution is to equip all sensors with Global Positioning Systems (GPS) [13]. However, this solution is impractical in indoor applications where GPS signals are not reliable. Alternative solutions define two types of sensors: *anchors* and *non-anchor nodes*. Anchors are sensors having known positions, whereas non-anchor nodes, or simply nodes, are unaware of their locations and hence they need to be localized. Generally, anchors are either static, having predefined positions, or mobile but tracked or moved by the user. The existing anchor-based algorithms could be divided into two categories: range-based and range-free algorithms. Range-based schemes consist of estimating the distances separating the nodes from anchors, and then combining these distances. Four distance estimation techniques have been mainly considered, using Time Of Arrival (TOA) [14], Time Difference Of Arrival (TDOA) [15], Angle Of Arrival (AOA) [16], or Received Signal Strength Indicator (RSSI) [11], [12]. TOA-based methods measure the travel times of signals exchanged between the sensors, whereas TDOA and AOA methods measure the difference of arrival times or the angles at reception of exchanged signals. While TOA, TDOA and AOA-based methods need extra hardware such as timers and synchronous clocks, RSSI-based methods are simpler, inexpensive and less-energy consuming using only powers of exchanged signals, but they are more challenging because of the reflection, the diffraction and the scattering of signals.

The alternative category to range-based localization consists of range-free algorithms. These techniques yield coarse-grained location estimates, leading to more than one possible solution to the problem. In this category, one could refer to connectivity-based techniques, where RSSI is compared to a strength threshold leading to bounds over distances [8]. Other range-free techniques are based on hop counts between anchors and nodes. Having per-hop distance, obtained through anchors communication, one could estimate the distances separating nodes from anchors [17], [18]. Distances information are then combined using different computation techniques, such as the Robust Optimization approach [19], the particle filter based on Monte-Carlo [7], the variational filter [20], interval analysis [21], Sigma-Point Kalman Smoothers as in [22], etc.

This paper considers the problem of localization in uncontrolled mobility sensor networks. The proposed technique is a range-free anchor-based method. Using connectivity measurements, the proposed method also takes advantage of the mobility of the nodes to set the problem. The novelty of this method is to use polar intervals to solve the problem. Indeed, position estimation is performed using polar coordinates in the interval framework. Estimates are thus partial rings, called polar boxes, enclosing the exact solution of the problem. Based on interval analysis [23], computation is handled in four different polar coordinate systems, leading to four position estimates at each time-step. Only one polar box is then selected at a considered step. It corresponds to the estimate having the smallest area, being the solution encloser presenting the least incertitude. The three remaining polar boxes are also kept in the memory to be used in the following time-step computation. Simulation results using Matlab corroborate the efficiency of the proposed method compared to other methods, especially to those handling computation in a single coordinate system.

The rest of the paper is organized as follows. Section II introduces the localization problem. Section III describes the proposed algorithm to solve the problem. Simulation results are given in Section IV whereas Section V concludes the paper.

F. Mourad, P. Honeine and H. Snoussi are with the Institut Charles Delaunay (ICD, UMR STMR CNRS 6279), Université de Technologie de Troyes, 12, rue Marie Curie, CS 42060, 10004 Troyes cedex, France, e-mail: {farah.mourad,paul.honeine,hichem.snoussi}@utt.fr.

II. Problem statement

Assume that the network is composed of N_a anchors and N_u nodes, deployed in a two-dimensional square area, denoted by Ω and having u_0 as side lengths. Let $\boldsymbol{a}_{i,t}$, $i \in \{1, ..., N_a\}$, and $\boldsymbol{u}_{j,t}$, $j \in \{1, ..., N_u\}$, be the respective positions of these sensors at time t. The aim of the method is to estimate all $\boldsymbol{u}_{j,t}$ positions using $\boldsymbol{a}_{i,t}$ information, as well as previous estimates. In order to reduce the communication costs, one assumes that nodes exchange information only with anchors. For this reason and without loss of generality, only one node $\boldsymbol{u}_t$ is considered in this paper and the index j is withdrawn. This paper handles computation using polar coordinates of sensors. In other words, the aim of the method is to estimate the polar coordinates of the node using the polar coordinates of some anchors. For this reason, one Polar Coordinate System (PCS), denoted by PCS$^{\llcorner}$, is first considered. Without loss of generality, the origin O$^{\llcorner}$ of PCS$^{\llcorner}$ is located at the low-left corner of the surveillance area Ω. An illustration is shown in Fig. 1. Here, the sensors polar coordinates are given by $\boldsymbol{a}^{\llcorner}_{i,t} = \left(\rho^{\llcorner}_{i,t}, \theta^{\llcorner}_{i,t}\right)$ and $\boldsymbol{u}^{\llcorner}_t = (\rho^{\llcorner}_t, \theta^{\llcorner}_t)$, where $\rho^{\llcorner}$ denotes the distance from the origin O$^{\llcorner}$ to the sensor and $\theta^{\llcorner}$ denotes the angle measured anticlockwise from the horizontal x-axis to the line joining O$^{\llcorner}$ to the sensor. According to this definition, $\theta^{\llcorner}_{i,t} \in [0, \frac{\pi}{2}]$, $\theta^{\llcorner}_t \in [0, \frac{\pi}{2}]$, $\rho^{\llcorner}_{i,t} \in [0, \rho_m]$ and $\rho^{\llcorner}_t \in [0, \rho_m]$, where $\rho_m = \sqrt{2}.u_0$ is the length of the diagonal of the surveillance area. It is worth noting that an infinite number of PCSs could be considered to define the localization problem. In the following, the localization problem is first described in PCS$^{\llcorner}$, and afterwards, it is reformulated in other PCSs.

A. Problem statement in PCS$^{\llcorner}$

The proposed method takes advantage of the mobility of the node to estimate nodes positions. The localization problem is thus defined using a mobility model, in addition to observation constraints. Any available information about the mobility of the node could be used to set the mobility constraints. This paper considers a general model assuming that the maximal velocity of the node is known and denoted by v_m. If Δt is the localization period, then the maximal distance that could be traveled by the node between two consecutive time-steps is equal to $D_m = \Delta t.v_m$. The mobility constraint is then given by the following,

$$d_t \leq D_m, \tag{1}$$

where d_t is the value of the distance traveled by the node between time-steps $t-1$ and t. Let $\boldsymbol{u}^{\llcorner}_{t-1} = \left(\rho^{\llcorner}_{t-1}, \theta^{\llcorner}_{t-1}\right)$ be the position of the node in PCS$^{\llcorner}$ at time $t-1$. Then d_t expressed in PCS$^{\llcorner}$ is the length of the side $\boldsymbol{u}^{\llcorner}_{t-1}\boldsymbol{u}^{\llcorner}_t$ of the triangle having the origin O$^{\llcorner}$, $\boldsymbol{u}^{\llcorner}_t$ and $\boldsymbol{u}^{\llcorner}_{t-1}$ as vertices. In this triangle, the lengths of O$^{\llcorner}\boldsymbol{u}^{\llcorner}_t$ and O$^{\llcorner}\boldsymbol{u}^{\llcorner}_{t-1}$ are given by $\rho^{\llcorner}_t$ and $\rho^{\llcorner}_{t-1}$ respectively, as shown in Fig. 1. The distance d_t could then be computed using the generalized Pythagorean theorem as follows,

$$d_t^2 = {\rho^{\llcorner}_t}^2 + {\rho^{\llcorner}_{t-1}}^2 - 2\rho^{\llcorner}_t\rho^{\llcorner}_{t-1}\cos\left(\theta^{\llcorner}_t - \theta^{\llcorner}_{t-1}\right), \tag{2}$$

where $|\theta^{\llcorner}_t - \theta^{\llcorner}_{t-1}|$ is the angle measured at the vertex O$^{\llcorner}$ in the considered triangle. The mobility constraint is then rewritten as follows,

$$ {\rho^{\llcorner}_t}^2 + {\rho^{\llcorner}_{t-1}}^2 - 2\rho^{\llcorner}_t\rho^{\llcorner}_{t-1}\cos\left(\theta^{\llcorner}_t - \theta^{\llcorner}_{t-1}\right) \leq D_m^2. \tag{3}$$

Graphically, this constraint yields a disk, called mobility disk, having the previous position as center and D_m as radius.

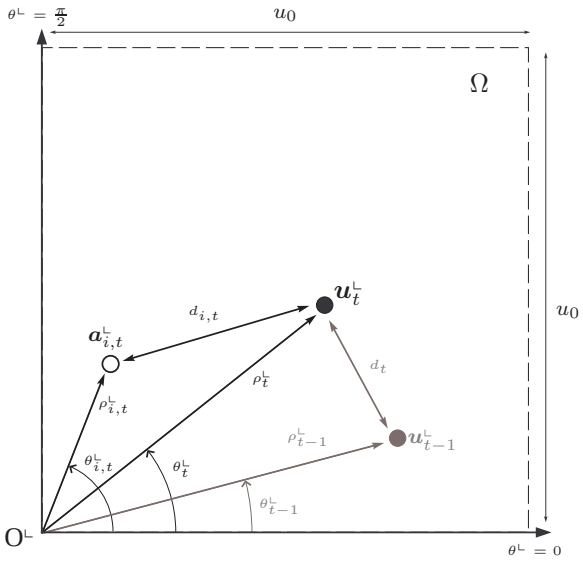

Fig. 1. Polar coordinates in PCS$^{\llcorner}$.

In addition to the mobility model, the proposed method is a range-free method based on RSSI information. At each time step, every anchor broadcasts signals in the network with the same initial power. According to the Okumura-Hata model [24], the strengths of the signals decrease monotonically with the increase of their traveled distances as follows,

$$\xi_{i,t} = \xi_0 \left(\frac{d_0}{d_{i,t}}\right)^{\alpha}, \tag{4}$$

where $\xi_{i,t}$ is the strength of the signal emitted by the anchor i and received by the mobile node at time t, ξ_0 is the strength measured at a reference distance d_0 from the anchor i, $d_{i,t}$ is the Euclidian distance between the anchor i and the node at time t and α is the path loss exponent. In practice, the RSSI of a signal could be modified due to the reflection, the diffraction or the scattering of the signal. Moreover the values of ξ_0 and α may vary from an anchor to the other. This may lead to inaccurate distances estimates. For this reason, the proposed method uses connectivity information, instead of using distances estimates. In other words, received strength values are only used to be compared to a threshold ξ_r, corresponding to the sensing range r of the sensors. If $\xi_{i,t} \geq \xi_r$, the anchor i is assumed to be within the sensing range of the node at time t. Otherwise, the anchor i is assumed to be too far and its information is not used. Connectivity measurements are then one-bit information generated as follows,

$$z_{i,t} = \begin{cases} 1 & \text{if } \xi_{i,t} \geq \xi_r \\ 0 & \text{otherwise} \end{cases}, \quad i \in \{1, ..., N_a\}. \tag{5}$$

Let I_t be the set of indices of all anchors having $z_{i,t} = 1$ at time t. The anchors denoted in I_t are assumed to be within

the sensing range of the node, and thus they are located at distances from the node less than r,

$$\forall i \in I_t,\ d_{i,t} \leq r. \tag{6}$$

One could obtain the expression of the distance $d_{i,t}$ between the anchor i and the considered node in PCS$^{\llcorner}$ by considering the triangle having the origin O$^{\llcorner}$, $\boldsymbol{a}^{\llcorner}_{i,t}$ and $\boldsymbol{u}^{\llcorner}_t$ as vertices, as shown in Fig. 1. The lengths of the sides O$^{\llcorner}\boldsymbol{u}^{\llcorner}_t$ and O$^{\llcorner}\boldsymbol{a}^{\llcorner}_{i,t}$ are given by $\rho^{\llcorner}_t$ and $\rho^{\llcorner}_{i,t}$ respectively, whereas $d_{i,t}$ is the length of the side $\boldsymbol{u}^{\llcorner}_t\boldsymbol{a}^{\llcorner}_{i,t}$ in the triangle. $d_{i,t}$ could then be computed using the generalized Pythagorean theorem as follows,

$$d^2_{i,t} = {\rho^{\llcorner}_t}^2 + {\rho^{\llcorner}_{i,t}}^2 - 2\rho^{\llcorner}_t\rho^{\llcorner}_{i,t}\cos\left(\theta^{\llcorner}_t - \theta^{\llcorner}_{i,t}\right), \tag{7}$$

with $|\theta^{\llcorner}_t - \theta^{\llcorner}_{i,t}|$ being the angle measured at the vertex O$^{\llcorner}$ in the considered triangle. The observation constraints are thus rewritten as follows,

$${\rho^{\llcorner}_t}^2 + {\rho^{\llcorner}_{i,t}}^2 - 2\rho^{\llcorner}_t\rho^{\llcorner}_{i,t}\cos\left(\theta^{\llcorner}_t - \theta^{\llcorner}_{i,t}\right) \leq r^2,\ i \in I_t. \tag{8}$$

This leads to a set of disks, called observation disks, having the detected anchors as centers and the communication range r as radii.

The localization problem is then defined in the considered PCS by both the mobility and the observation models as follows,

$$\left|\begin{array}{l} {\rho^{\llcorner}_t}^2 + {\rho^{\llcorner}_{t-1}}^2 - 2\rho^{\llcorner}_t\rho^{\llcorner}_{t-1}\cos\left(\theta^{\llcorner}_t - \theta^{\llcorner}_{t-1}\right) \leq D^2_m, \\ {\rho^{\llcorner}_t}^2 + {\rho^{\llcorner}_{i,t}}^2 - 2\rho^{\llcorner}_t\rho^{\llcorner}_{i,t}\cos\left(\theta^{\llcorner}_t - \theta^{\llcorner}_{i,t}\right) \leq r^2,\ i \in I_t, \\ \rho^{\llcorner}_t \in [0, \rho_m], \quad \theta^{\llcorner}_t \in [0, \frac{\pi}{2}], \end{array}\right. \tag{9}$$

where $\rho^{\llcorner}_{i,t}$, $\theta^{\llcorner}_{i,t}$, $i \in I_t$, r, D_m and ρ_m have known values, and $\rho^{\llcorner}_{t-1}$ and $\theta^{\llcorner}_{t-1}$ are estimated at time $t-1$. Graphically, the problem at a given time t consists of overlapping the mobility disk, centered on the previous position and having D_m as radius, with a set of observation disks, having r as radii and the detected anchors as centers. An example of such a problem with three detected anchors is shown in Fig. 2. The solution of the problem is given by the overlapping area of all disks, as shown in dark gray in the plot.

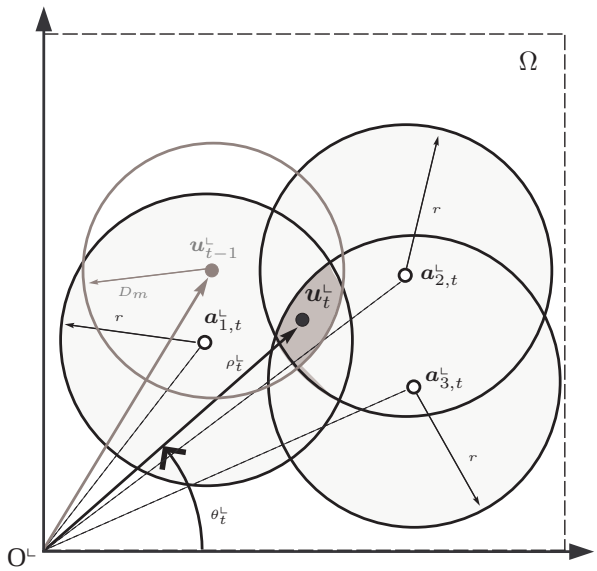

Fig. 2. An example of a localization problem in PCS$^{\llcorner}$ at time t.

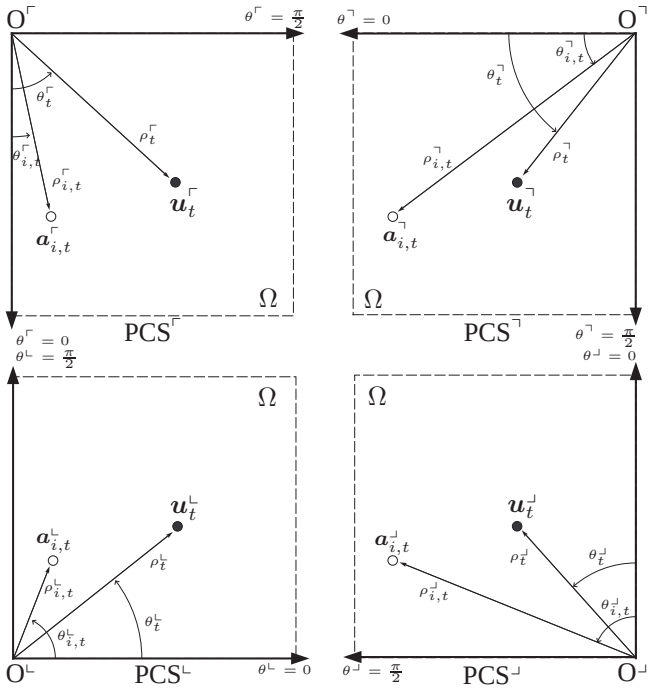

Fig. 3. Polar coordinates in four different PCSs.

B. Problem statement in several PCSs

In the previous section, the localization problem is defined in a specific PCS, denoted by PCS$^{\llcorner}$, having its origin O$^{\llcorner}$ at the low-left corner of Ω. In PCS$^{\llcorner}$, all distances to the origin $\rho^{\llcorner}$ are included in $[0, \rho_m]$ and all angles $\theta^{\llcorner}$ are included in $[0, \frac{\pi}{2}]$. One could define the localization problem in an infinite number of PCSs over the surveillance area Ω. However, only three PCSs other than PCS$^{\llcorner}$ could be set with $\rho \in [0, \rho_m]$ and $\theta \in [0, \frac{\pi}{2}]$. These PCSs, denoted by PCS$^{\lrcorner}$, PCS$^{\urcorner}$ and PCS$^{\ulcorner}$, have their respective origins O$^{\lrcorner}$, O$^{\urcorner}$ and O$^{\ulcorner}$ at the low-right, the up-right and the up-left corners of Ω respectively. Also, they are rotated anticlockwise respectively by angles of $\frac{\pi}{2}$, π and $\frac{3\pi}{2}$ with respect to PCS$^{\llcorner}$. An illustration of these PCSs is given in Fig. 3. According to this definition, the bounds over the distances to origins and the angles remain unchanged. Observation and mobility constraints are also valid, which leads to the following formulation of the localization problem in any of these PCSs,

$$\left|\begin{array}{l} {\rho^{\diamond}_t}^2 + {\rho^{\diamond}_{t-1}}^2 - 2\rho^{\diamond}_t\rho^{\diamond}_{t-1}\cos\left(\theta^{\diamond}_t - \theta^{\diamond}_{t-1}\right) \leq D^2_m, \\ {\rho^{\diamond}_t}^2 + {\rho^{\diamond}_{i,t}}^2 - 2\rho^{\diamond}_t\rho^{\diamond}_{i,t}\cos\left(\theta^{\diamond}_t - \theta^{\diamond}_{i,t}\right) \leq r^2,\ i \in I_t, \\ \rho^{\diamond}_t \in [0, \rho_m], \quad \theta^{\diamond}_t \in [0, \frac{\pi}{2}], \end{array}\right. \tag{10}$$

where the superindex $\diamond \in \{\llcorner, \lrcorner, \urcorner, \ulcorner\}$, r and D_m are known, $\rho^{\diamond}_{i,t}$ and $\theta^{\diamond}_{i,t}$ are anchors coordinates expressed differently in the given PCSs and $\rho^{\diamond}_{t-1}$ and $\theta^{\diamond}_{t-1}$ are estimated at time $t-1$, each in its corresponding PCS. Assume that anchors coordinates are given in the first PCS, denoted by PCS$^{\llcorner}$. One could deduce geometrically the expressions of these

TABLE I
GLOSSARY OF TERMS.

Terms	Definitions
$\diamond$	Designation of the considered PCS, $\diamond \in \{\llcorner, \lrcorner, \urcorner, \ulcorner\}$
$\rho_t^\diamond$	1st polar coordinate of the node in PCS$^\diamond$ at time t
$\theta_t^\diamond$	2nd polar coordinate of the node in PCS$^\diamond$ at time t
$\boldsymbol{u}_t^\diamond$	Polar coordinates vector of the node in PCS$^\diamond$ at time t
$\rho_{i,t}^\diamond$	1st polar coordinate of the anchor i in PCS$^\diamond$ at time t
$\theta_{i,t}^\diamond$	2nd polar coordinate of the anchor i in PCS$^\diamond$ at time t
$\boldsymbol{a}_{i,t}^\diamond$	Polar coordinates vector of the anchor i in PCS$^\diamond$ at time t
D_m	Maximal distance traveled by the node
r	Communication range
ρ_m	Length of the diagonal of the surveillance area
u_0	Length of a side of the surveillance area

coordinates in the remaining PCSs as follows,

$$\left|\begin{array}{l} \rho_{i,t}^{\lrcorner} = \sqrt{{\rho_{i,t}^{\llcorner}}^2 + u_0^2 - 2\rho_{i,t}^{\llcorner} u_0 \cos\left(\theta_{i,t}^{\llcorner}\right)}, \\ \theta_{i,t}^{\lrcorner} = \arctan \frac{u_0 - \rho_{i,t}^{\llcorner}\cos\left(\theta_{i,t}^{\llcorner}\right)}{\rho_{i,t}^{\llcorner}\sin\left(\theta_{i,t}^{\llcorner}\right)}, \end{array}\right.$$

$$\left|\begin{array}{l} \rho_{i,t}^{\urcorner} = \sqrt{{\rho_{i,t}^{\llcorner}}^2 + 2u_0^2 - 2\rho_{i,t}^{\llcorner} u_0 \left(\cos\left(\theta_{i,t}^{\llcorner}\right) + \sin\left(\theta_{i,t}^{\llcorner}\right)\right)}, \\ \theta_{i,t}^{\urcorner} = \arctan \frac{u_0 - \rho_{i,t}^{\llcorner}\sin\left(\theta_{i,t}^{\llcorner}\right)}{u_0 - \rho_{i,t}^{\llcorner}\cos\left(\theta_{i,t}^{\llcorner}\right)}, \end{array}\right.$$

$$\left|\begin{array}{l} \rho_{i,t}^{\ulcorner} = \sqrt{{\rho_{i,t}^{\llcorner}}^2 + u_0^2 - 2\rho_{i,t}^{\llcorner} u_0 \sin\left(\theta_{i,t}^{\llcorner}\right)}, \\ \theta_{i,t}^{\ulcorner} = \arctan \frac{\rho_{i,t}^{\llcorner}\cos\left(\theta_{i,t}^{\llcorner}\right)}{u_0 - \rho_{i,t}^{\llcorner}\sin\left(\theta_{i,t}^{\llcorner}\right)}. \end{array}\right. \tag{11}$$

Once the localization problem is set in PCS$^\llcorner$, PCS$^\lrcorner$, PCS$^\urcorner$ and PCS$^\ulcorner$, one could choose a single PCS among these four PCSs to solve the problem. Another way to handle the problem consists of performing computation in all the defined PCSs and then select the best resulting solution, as it is shown in the following section. A glossary of all terms is given in TABLE I.

III. POLAR-INTERVAL LOCALIZATION ALGORITHM

Solving the localization problem consists of estimating the coordinates of the considered node at each time step, given the constraints of (10). One could choose a single PCS, for instance PCS$^\llcorner$, to compute the solution. In a different manner, this paper proposes to handle the problem in all defined PCSs and then choosing the best solution between the resulting ones. Computation is thus performed in each PCS of PCS$^\llcorner$, PCS$^\lrcorner$, PCS$^\urcorner$ and PCS$^\ulcorner$, leading to four estimates of the position of the node at each time-step. In the following, the proposed method, based on interval analysis [23], is first described, and then the localization algorithm is presented.

A. Description of the method

The solution of the problem is proposed using interval analysis [23]. Instead of computing an exact position estimate at each time step, the method consists of performing an outer estimation of the solution. In other words, it aims at bounding the coordinates of the node, in the way to cover all possible solutions of the problem. Consider that computation is performed in a specific PCS, denoted by PCS$^\diamond$ with $\diamond \in \{\llcorner, \lrcorner, \urcorner, \ulcorner\}$. The solution is then given by a two-dimensional interval, denoted by $[\boldsymbol{u}_t^\diamond]$. Also called polar box, $[\boldsymbol{u}_t^\diamond]$ is defined by the cartesian product of two real intervals $[\rho_t^\diamond]$ and $[\theta_t^\diamond]$, defined over the polar coordinates $\rho_t^\diamond$ and $\theta_t^\diamond$ respectively,

$$[\boldsymbol{u}_t^\diamond] = [\rho_t^\diamond] \times [\theta_t^\diamond] = [\underline{\rho_t^\diamond}, \overline{\rho_t^\diamond}] \times [\underline{\theta_t^\diamond}, \overline{\theta_t^\diamond}], \tag{12}$$

where $\underline{\rho_t^\diamond} = \inf\left([\rho_t^\diamond]\right)$ and $\overline{\rho_t^\diamond} = \sup\left([\rho_t^\diamond]\right)$ denote respectively the lower and the higher endpoints of the real interval $[\rho_t^\diamond]$ and $\underline{\theta_t^\diamond} = \inf\left([\theta_t^\diamond]\right)$ and $\overline{\theta_t^\diamond} = \sup\left([\theta_t^\diamond]\right)$ denote respectively the lower and the higher endpoints of the real interval $[\theta_t^\diamond]$. Having the localization problem of (10) at time t, solving the problem consists of finding the minimal polar box $[\boldsymbol{u}_t^\diamond]$ including all possible solutions. Starting with an initial box $[\boldsymbol{u}]_0$, the proposed method aims at minimizing the widths $\left(\overline{\rho_t^\diamond} - \underline{\rho_t^\diamond}\right)$ and $\left(\overline{\theta_t^\diamond} - \underline{\theta_t^\diamond}\right)$ of $[\rho_t^\diamond]$ and $[\theta_t^\diamond]$ respectively according to the constraints of (10). The initial polar box $[\boldsymbol{u}]_0$ could be defined by $[0, \rho_m] \times [0, \frac{\pi}{2}]$, since $\rho_t^\diamond \in [0, \rho_m]$ and $\theta_t^\diamond \in [0, \frac{\pi}{2}]$ as shown in Section II.

Graphically, the solution box is a partial ring, having the origin O$^\diamond$ of the considered PCS as center and $\underline{\rho_t^\diamond}$ and $\overline{\rho_t^\diamond}$ as inner and outer radii respectively. Moreover, it is defined between the lines starting at the origin and having $\underline{\theta_t^\diamond}$ and $\overline{\theta_t^\diamond}$ as angles. The best solution box corresponding to the problem of Fig. 2 is given in thick black line in Fig. 4. Here the illustration is shown in PCS$^\llcorner$ and the previous estimate is assumed to be exact. In fact, according to the proposed method, the previous estimate is a polar box denoted by $[\boldsymbol{u}_{t-1}^\llcorner]$. Propagating $[\boldsymbol{u}_{t-1}^\llcorner]$ using the mobility disk leads to a larger domain, defined by the union of all the disks obtained by the propagation of each point of $[\boldsymbol{u}_{t-1}^\llcorner]$ with the mobility model. An illustration of this domain, called mobility domain, is given in Fig. 5. Actually, instead of using the mobility disk as in Fig. 4 and since the previous solution is a box, one should overlap the mobility domain with the observation disks to define the solution polar box in the considered PCS. An illustration of the solution box of PCS$^\llcorner$ is given in black in Fig. 6. It is clear that this box is larger than the one illustrated in Fig. 4. This way the resulting box is guaranteed to contain the exact solution of the problem since it takes previous and actual incertitude into consideration.

Fig. 7 illustrates the polar boxes obtained in PCS$^\llcorner$, PCS$^\lrcorner$, PCS$^\urcorner$ and PCS$^\ulcorner$. Here the previous estimates are assumed to be exact for simplicity of illustration. In fact, for each PCS of superindex $\diamond \in \{\llcorner, \lrcorner, \urcorner, \ulcorner\}$, the corresponding previous polar box $[\boldsymbol{u}_{t-1}^\diamond]$ should be employed to compute the actual estimate $[\boldsymbol{u}_t^\diamond]$. Once the four estimates are obtained, areas of these estimates are computed as follows,

$$\mathbf{Ar}\left([\boldsymbol{u}_t^\diamond]\right) = \frac{\left(\overline{\theta_t^\diamond} - \underline{\theta_t^\diamond}\right)\left(\overline{\rho_t^\diamond}^2 - \underline{\rho_t^\diamond}^2\right)}{2}, \tag{13}$$

where $[\boldsymbol{u}_t^\diamond] = [\underline{\rho_t^\diamond}, \overline{\rho_t^\diamond}] \times [\underline{\theta_t^\diamond}, \overline{\theta_t^\diamond}]$. The values of these areas represent the incertitude obtained while computing the minimal encloser of the solution in the corresponding PCS. For this reason, and since all computed boxes include the solution area of the problem, the polar box having the minimal area is selected to be the solution box at the considered time-step.

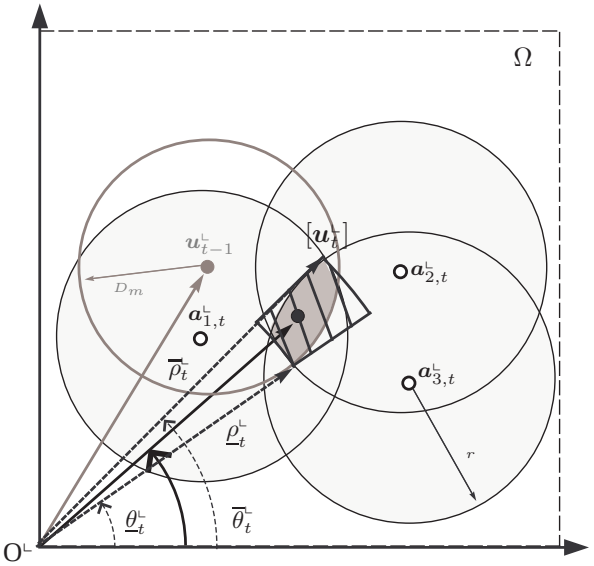

Fig. 4. Polar box obtained in PCS$^{\llcorner}$ for the problem of Fig. 2 with an exact previous estimate.

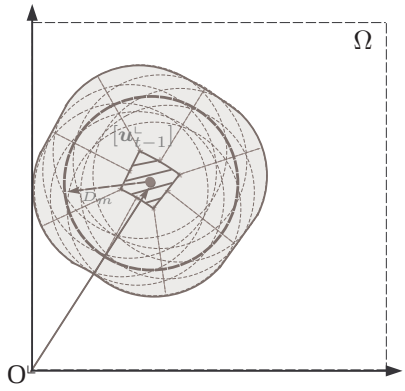

Fig. 5. Propagation of the previous polar box using the mobility model.

The three remaining boxes are also kept in the memory to be used with the mobility model in the following time-step.

B. Proposed algorithm

Consider the problem of (10) defined in one PCS, denoted by PCS$^{\diamond}$, $\diamond \in \{\llcorner, \lrcorner, \urcorner, \ulcorner\}$. In order to compute the solution box $[\boldsymbol{u}_t^{\diamond}]$ at a given time t, one should set all available constraints on $\rho_t^{\diamond}$ and $\theta_t^{\diamond}$ according to (10). The first general constraints to be set are given by the dimensions of the surveillance area,

$$0 \leq \rho_t^{\diamond} \leq \rho_m \quad \text{and} \quad 0 \leq \theta_t^{\diamond} \leq \frac{\pi}{2}. \tag{14}$$

Moreover, since the cosine of an angle is always less than 1 and $\rho_t^{\diamond}$ and $\rho_{i,t}^{\diamond}$ are always positive for $i \in I_t$, then $\left(\rho_t^{\diamond} - \rho_{i,t}^{\diamond}\right)^2 \leq {\rho_t^{\diamond}}^2 + {\rho_{i,t}^{\diamond}}^2 - 2\rho_t^{\diamond}\rho_{i,t}^{\diamond}\cos\left(\theta_t^{\diamond} - \theta_{i,t}^{\diamond}\right)$. Hence, each observation constraint of (10), for $i \in I_t$, leads to the following constraint,

$$\left(\rho_t^{\diamond} - \rho_{i,t}^{\diamond}\right)^2 \leq r^2 \Leftrightarrow \rho_{i,t}^{\diamond} - r \leq \rho_t^{\diamond} \leq \rho_{i,t}^{\diamond} + r. \tag{15}$$

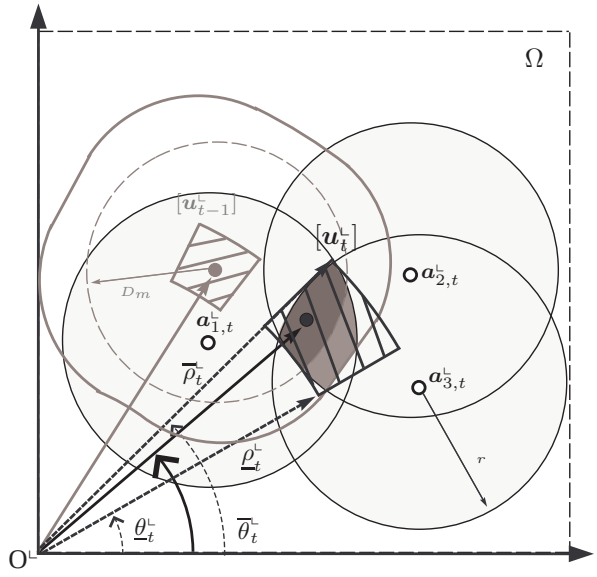

Fig. 6. Polar box obtained in PCS$^{\llcorner}$ for the problem of Fig. 2 taking the previous polar box into consideration.

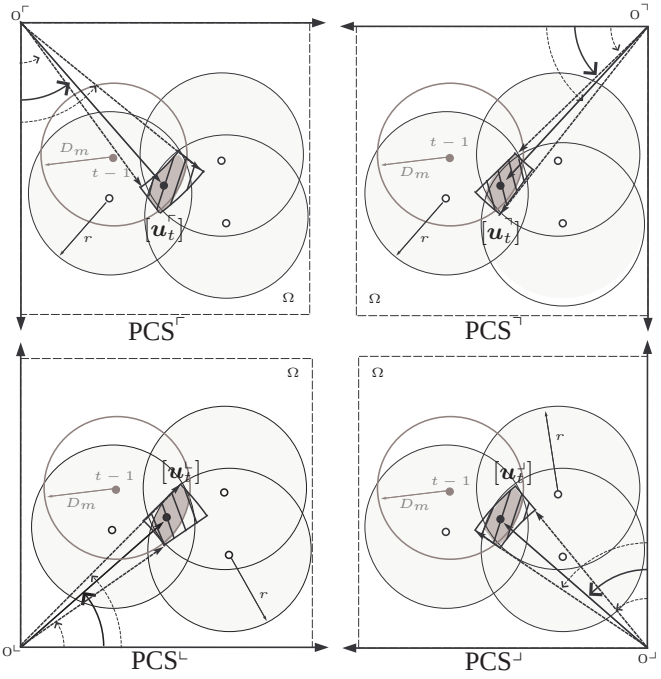

Fig. 7. Solutions of the problem in the four predefined PCSs.

In the same manner, the mobility constraint leads to the following,

$$\rho_{t-1}^{\diamond} - D_m \leq \rho_t^{\diamond} \leq \rho_{t-1}^{\diamond} + D_m, \tag{16}$$

where the exact value of $\rho_{t-1}^{\diamond}$ is unknown, but according to the previous description, $\rho_{t-1}^{\diamond} \in [\rho_{t-1}^{\diamond}]$ with $[\rho_{t-1}^{\diamond}] = [\underline{\rho}_{t-1}^{\diamond}, \overline{\rho}_{t-1}^{\diamond}]$. Then,

$$\underline{\rho}_{t-1}^{\diamond} - D_m \leq \rho_t^{\diamond} \leq \overline{\rho}_{t-1}^{\diamond} + D_m. \tag{17}$$

Combining all constraints over $\rho_t^\diamond$ leads then to the following,

$$\begin{aligned}\max\left(0, \underline{\rho}_{t-1}^\diamond - D_m, \max_{i\in I_t}\left(\rho_{i,t}^\diamond - r\right)\right) \leq \rho_t^\diamond \dashrightarrow \\ \leq \min\left(\rho_m, \overline{\rho}_{t-1}^\diamond + D_m, \min_{i\in I_t}\left(\rho_{i,t}^\diamond + r\right)\right).\end{aligned} \tag{18}$$

On the other hand,

$$\begin{aligned}{\rho_t^\diamond}^2 + {\rho_{i,t}^\diamond}^2 - 2\rho_t^\diamond\rho_{i,t}^\diamond\cos\left(\theta_t^\diamond - \theta_{i,t}^\diamond\right) \dashrightarrow \\ \left(\rho_t^\diamond - \rho_{i,t}^\diamond\cos\left(\theta_t^\diamond - \theta_{i,t}^\diamond\right)\right)^2 + {\rho_{i,t}^\diamond}^2\sin^2\left(\theta_t^\diamond - \theta_{i,t}^\diamond\right).\end{aligned} \tag{19}$$

Then each observation constraint of (10) leads inevitably to the following,

$${\rho_{i,t}^\diamond}^2\sin^2\left(\theta_t^\diamond - \theta_{i,t}^\diamond\right) \leq r^2 \Leftrightarrow -\frac{r}{\rho_{i,t}^\diamond} \leq \sin\left(\theta_t^\diamond - \theta_{i,t}^\diamond\right) \leq \frac{r}{\rho_{i,t}^\diamond}. \tag{20}$$

If $\frac{r}{\rho_{i,t}^\diamond} \leq 1$, for $i \in I_t$, and since $\left(\theta_t^\diamond - \theta_{i,t}^\diamond\right) \in [-\frac{\pi}{2}, \frac{\pi}{2}]$ where the sine function is monotonically increasing, the previous constraint leads to

$$\theta_{i,t}^\diamond - \arcsin^*\left(\frac{r}{\rho_{i,t}^\diamond}\right) \leq \theta_t^\diamond \leq \theta_{i,t}^\diamond + \arcsin^*\left(\frac{r}{\rho_{i,t}^\diamond}\right), \tag{21}$$

where $\arcsin^*(x) = \arcsin(\min(1, x))$. In the same manner, the mobility constraint leads to the following,

$$\theta_{t-1}^\diamond - \arcsin^*\left(\frac{D_m}{\rho_{t-1}^\diamond}\right) \leq \theta_t^\diamond \leq \theta_{t-1}^\diamond + \arcsin^*\left(\frac{D_m}{\rho_{t-1}^\diamond}\right). \tag{22}$$

Since $\rho_{t-1}^\diamond \in [\rho_{t-1}^\diamond]$ and $\theta_{t-1}^\diamond \in [\theta_{t-1}^\diamond]$ with $[\rho_{t-1}^\diamond] = [\underline{\rho}_{t-1}^\diamond, \overline{\rho}_{t-1}^\diamond]$ and $[\theta_{t-1}^\diamond] = [\underline{\theta}_{t-1}^\diamond, \overline{\theta}_{t-1}^\diamond]$, and since the arcsine function is monotonically increasing on the considered domain, then

$$\underline{\theta}_{t-1}^\diamond - \arcsin^*\left(\frac{D_m}{\underline{\rho}_{t-1}^\diamond}\right) \leq \theta_t^\diamond \leq \overline{\theta}_{t-1}^\diamond + \arcsin^*\left(\frac{D_m}{\underline{\rho}_{t-1}^\diamond}\right). \tag{23}$$

Combining all constraints over $\theta_t^\diamond$ leads then to the following,

$$\begin{aligned}\max\left(0, \underline{\theta}_{t-1}^\diamond - \arcsin^*\left(\frac{D_m}{\underline{\rho}_{t-1}^\diamond}\right), \max_{i\in I_t}\left(\theta_{i,t}^\diamond - \arcsin^*\left(\frac{r}{\rho_{i,t}^\diamond}\right)\right)\right) \leq \theta_t^\diamond \dashrightarrow \\ \leq \min\left(\frac{\pi}{2}, \overline{\theta}_{t-1}^\diamond + \arcsin^*\left(\frac{D_m}{\underline{\rho}_{t-1}^\diamond}\right), \min_{i\in I_t}\left(\theta_{i,t}^\diamond + \arcsin^*\left(\frac{r}{\rho_{i,t}^\diamond}\right)\right)\right).\end{aligned} \tag{24}$$

One could then define the first solution box by

$$[\boldsymbol{u}_t^\diamond]^{(1)} = [\underline{\rho}_t^{\diamond(1)}, \overline{\rho}_t^{\diamond(1)}] \times [\underline{\theta}_t^{\diamond(1)}, \overline{\theta}_t^{\diamond(1)}], \tag{25}$$

with

$$\begin{aligned}\underline{\rho}_t^{\diamond(1)} &= \max\left(0, \underline{\rho}_{t-1}^\diamond - D_m, \max_{i\in I_t}\left(\rho_{i,t}^\diamond - r\right)\right), \\ \overline{\rho}_t^{\diamond(1)} &= \min\left(\rho_m, \overline{\rho}_{t-1}^\diamond + D_m, \min_{i\in I_t}\left(\rho_{i,t}^\diamond + r\right)\right), \\ \underline{\theta}_t^{\diamond(1)} &= \max\left(0, \underline{\theta}_{t-1}^\diamond - \arcsin^*\left(\frac{D_m}{\underline{\rho}_{t-1}^\diamond}\right), \max_{i\in I_t}\left(\theta_{i,t}^\diamond - \arcsin^*\left(\frac{r}{\rho_{i,t}^\diamond}\right)\right)\right), \\ \overline{\theta}_t^{\diamond(1)} &= \min\left(\frac{\pi}{2}, \overline{\theta}_{t-1}^\diamond + \arcsin^*\left(\frac{D_m}{\underline{\rho}_{t-1}^\diamond}\right), \min_{i\in I_t}\left(\theta_{i,t}^\diamond + \arcsin^*\left(\frac{r}{\rho_{i,t}^\diamond}\right)\right)\right).\end{aligned} \tag{26}$$

Fig. 8 shows in thick black line the first solution box $[\boldsymbol{u}_t^\diamond]^{(1)}$, obtained for the localization problem of Fig. 2, with $\diamond = \llcorner$. It is obvious that this box is not minimal. It is indeed larger than the solution box that should be obtained, as illustrated in Fig. 6. For this reason, one could set more constraints on $\rho_t^\diamond$ and $\theta_t^\diamond$, with bounds being functions of $\theta_t^\diamond$ and $\rho_t^\diamond$ respectively. Once $[\boldsymbol{u}_t^\diamond]^{(1)}$ is computed, these constraints could be used to contract it at maximal leading to the final solution box.

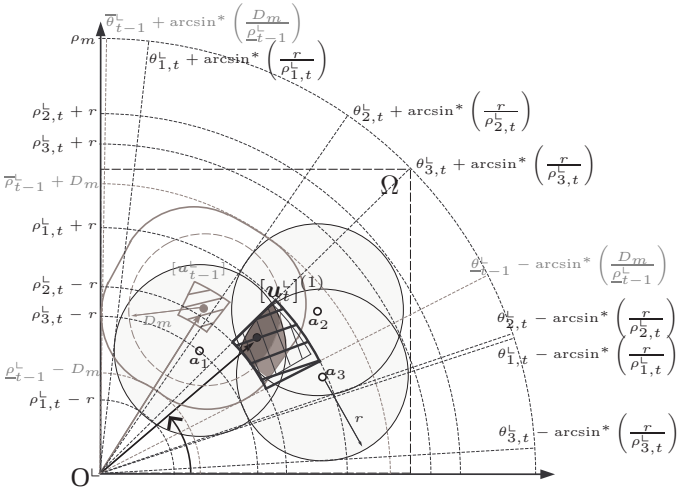

Fig. 8. First solution box obtained for the localization problem of Fig. 2 in PCS$^\llcorner$.

On the first hand, observation constraints of (10) and equation (19) lead to the following constraints with $i \in I_t$,

$$\begin{aligned}\rho_i^\diamond(t)\cos\left(\theta_t^\diamond - \theta_{i,t}^\diamond\right) - \sqrt{r^2 - {\rho_{i,t}^\diamond}^2\sin^2\left(\theta_t^\diamond - \theta_{i,t}^\diamond\right)} \leq \rho_t^\diamond \dashrightarrow \\ \leq \rho_{i,t}^\diamond\cos\left(\theta_t^\diamond - \theta_{i,t}^\diamond\right) + \sqrt{r^2 - {\rho_{i,t}^\diamond}^2\sin^2\left(\theta_t^\diamond - \theta_{i,t}^\diamond\right)}.\end{aligned} \tag{27}$$

In the same manner, the mobility constraint leads to the following,

$$\begin{aligned}\rho_{t-1}^\diamond\cos\left(\theta_t^\diamond - \theta_{t-1}^\diamond\right) - \sqrt{D_m^2 - {\rho_{t-1}^\diamond}^2\sin^2\left(\theta_t^\diamond - \theta_{t-1}^\diamond\right)} \leq \rho_t^\diamond \dashrightarrow \\ \leq \rho_{t-1}^\diamond\cos\left(\theta_t^\diamond - \theta_{t-1}^\diamond\right) + \sqrt{D_m^2 - {\rho_{t-1}^\diamond}^2\sin^2\left(\theta_t^\diamond - \theta_{t-1}^\diamond\right)},\end{aligned} \tag{28}$$

with $\rho_{t-1}^\diamond \in [\rho_{t-1}^\diamond]$ and $\theta_{t-1}^\diamond \in [\theta_{t-1}^\diamond]$.

On the second hand, observation constraints of (10) could be reformulated as follows,

$$\cos\left(\theta_t^\diamond - \theta_{i,t}^\diamond\right) \geq \frac{{\rho_t^\diamond}^2 + {\rho_{i,t}^\diamond}^2 - r^2}{2\rho_t^\diamond\rho_{i,t}^\diamond}. \tag{29}$$

Then,

$$\theta_{i,t}^\diamond - \arccos\left(\frac{{\rho_t^\diamond}^2 + {\rho_{i,t}^\diamond}^2 - r^2}{2\rho_t^\diamond\rho_{i,t}^\diamond}\right) \leq \theta_t^\diamond \leq \theta_{i,t}^\diamond + \arccos\left(\frac{{\rho_t^\diamond}^2 + {\rho_{i,t}^\diamond}^2 - r^2}{2\rho_t^\diamond\rho_{i,t}^\diamond}\right). \tag{30}$$

In the same manner, the mobility constraint leads to the following,

$$\theta_{t-1}^\diamond - \arccos\left(\frac{{\rho_t^\diamond}^2 + {\rho_{t-1}^\diamond}^2 - D_m^2}{2\rho_t^\diamond\rho_{t-1}^\diamond}\right) \leq \theta_t^\diamond \leq \theta_{t-1}^\diamond + \arccos\left(\frac{{\rho_t^\diamond}^2 + {\rho_{t-1}^\diamond}^2 - D_m^2}{2\rho_t^\diamond\rho_{t-1}^\diamond}\right), \tag{31}$$

with $\rho_{t-1}^\diamond \in [\rho_{t-1}^\diamond]$ and $\theta_{t-1}^\diamond \in [\theta_{t-1}^\diamond]$.

One could use bounds of $\theta_t^\diamond$ with (27) and (28) to compute new bounds of $\rho_t^\diamond$ and bounds of $\rho_t^\diamond$ with (30) and (31) to compute new bounds of $\theta_t^\diamond$, which might contract $[\boldsymbol{u}_t^\diamond]^{(1)}$. Practically, in order to contract the polar box $[\boldsymbol{u}_t^\diamond]^{(1)}$, the constraints of (27), (28), (30) and (31) are iterated in the interval framework using the forward-backward contractor [23], [8]. This contractor iterates all constraints, while using interval notations, without any prior order until no contraction is possible. The polar box obtained at time t using this contractor would be at best the box illustrated in Fig. 6, given

the problem of Fig. 2. It is worth noting that the computation is performed separately in the four PCSs, in order to select at last the resulting box having the minimal area. The proposed algorithm at a considered time t is given in appendix. If an exact estimate is needed, this estimate would correspond to the barycenter of the selected polar box at each time-step.

IV. Simulations

This section illustrates the performances of the proposed method, denoted PIL4 for *Polar Interval-based Localization using 4 PCSs*. For this aim, a single mobile node moving over $100s$ in a $100m \times 100m$ square area is considered. The maximal velocity of the node is set to its exact value, equal to $3.17m/s$, leading to a maximal distance of $3.17m$ with a localization period of $1s$. Anchors are assumed to be static either randomly or uniformly deployed over the surveillance area. The sensing area of the sensors is assumed to be circular with a $10m$ sensing range. It is worth noting that connectivity measurements at a given time step are generated by computing the distances between the mobile node and all anchors at this step and then setting to one the measurement corresponding to the anchor having a distance to the node less than $10m$. In the following, all simulations are performed on an Intel(R) Core(TM) i5-2520M CPU (2.5GHz, 4.00GB RAM) using MATLAB 7.10.0.499.

A. Comparison of PIL4 to a one-PCS-based method

This paragraph illustrates the effectiveness of the proposed method, compared to another version of the method, denoted PIL1, using only one PCS which is $\text{PCS}^{\llcorner}$. Here anchors are first randomly deployed with a density set to 0.015 anchor per m^2, leading to 150 anchors randomly deployed over the square area, as shown in Fig. 9. With a $10m$ circular sensing range, the node detects at average 5 anchors at each time step, with the number of detected anchors going from 1 to 11. Fig. 9 shows the polar boxes obtained using PIL4 in straight line and PIL1 in dashed line. The plot also shows the estimated exact positions with PIL4 given at the centers of the estimated boxes. Let the estimation errors be the distances separating the centers of the estimated boxes from the exact positions. Fig. 10 shows the ratios of the areas of the boxes obtained with PIL4 over those of PIL1 in the top plot and the ratios of estimation errors PIL4 over PIL1 in the bottom plot. As illustrated, the estimates of PIL4 are more accurate than those of PIL1. 150 anchors are then randomly deployed in 5 different manners. Both methods are then performed using these distributions and results are averaged over the 5 attempts in the following. TABLE II shows the average boxes areas, the average estimation errors and the average computation times per time-step obtained with PIL4 and PIL1. According to these results, using four PCSs leads to a decrease of around 22% of the boxes areas and 23% of the estimation errors. In other words, performing computation in more than one PCS leads to more accurate estimates with less incertitude, at the cost of the computation time that increases but remains negligible.

PIL4 is then compared to PIL1 with a different anchors configuration. Here anchors are assumed to be uniformly deployed with a density of 0.01 anchor per m^2, leading to 100 anchors regularly spaced over the surveillance area as shown in Fig. 13. With this configuration, the node detects at average 3.13 anchors per time-step with the number of detected anchors varying between 2 and 4 anchors. TABLE III shows the average boxes areas, the average estimation errors and the average computation times per time-step obtained with PIL4 and PIL1. According to these results, PIL4 remains more accurate than PIL1 but more time consuming. It is worth noting that the computation times here are less than the ones obtained above since less anchors are detected leading to less observation constraints at each time-step.

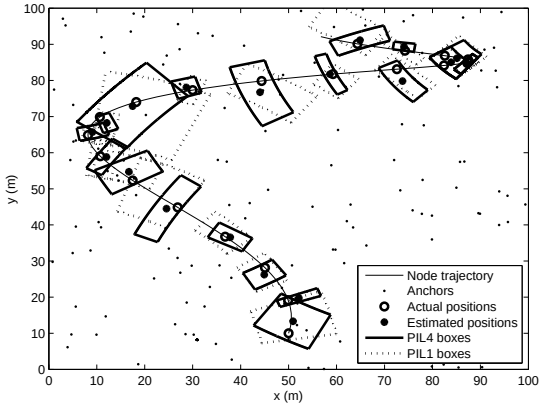

Fig. 9. Estimated boxes obtained using PIL4 and PIL1.

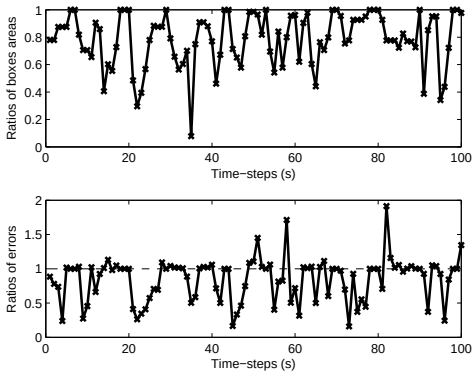

Fig. 10. Ratios of boxes areas PIL4/PIL1 in the top plot. Ratios of estimation errors PIL4/PIL1 in the bottom plot.

TABLE II
Comparison of PIL4 to PIL1 with randomly deployed anchors.

Methods	Boxes areas	Estimation errors	Computation times
PIL4	$64.44m^2$	$1.99m$	$0.0064s$
PIL1	$82.95m^2$	$2.59m$	$0.0032s$

TABLE III
Comparison of PIL4 to PIL1 with uniformly deployed anchors.

Methods	Boxes areas	Estimation errors	Computation times
PIL4	$59.77m^2$	$2.01m$	$0.0037s$
PIL1	$71.02m^2$	$2.21m$	$0.0016s$

TABLE IV
COMPARISON OF PIL4 TO PIL4O WITH RANDOMLY DEPLOYED ANCHORS.

Methods	Boxes areas	Estimation errors	Computation times
PIL4	$64.44m^2$	$1.99m$	$0.0064s$
PIL4o	$85.99m^2$	$2.67m$	$0.0067s$

TABLE V
COMPARISON OF PIL4 TO PIL4O WITH UNIFORMLY DEPLOYED ANCHORS.

Methods	Boxes areas	Estimation errors	Computation times
PIL4	$59.77m^2$	$2.01m$	$0.0037s$
PIL4o	$74.85m^2$	$2.26m$	$0.0038s$

B. Effectiveness of the mobility model

In this section, the proposed method is compared to another version of the method using only the observation constraints, denoted PIL4o. 150 anchors are first randomly deployed in the surveillance area in 5 different manners. TABLE IV shows the computation results obtained with both methods averaged over the 5 attempts. As expected, the use of the mobility model increases the accuracy of the estimation. 100 uniformly deployed anchors are then considered. TABLE V shows the results obtained with both methods. Here also using the mobility model reduces the incertitude of estimation. Indeed, with the mobility model, the mobility domain is overlapped with the intersection area of observation disks, which reduces the resulting box as shown for instance in Fig. 11. While PIL4o yields the smallest polar box covering the intersection of the observation disks, PIL4 yields a smaller box reduced by the mobility domain. It is worth noting that the mobility box illustrated in gray in the plot corresponds to the polar box covering the exact mobility domain.

C. Effectiveness of the contraction phase

In this section, the proposed method PIL4 is compared to its relaxed version, denoted PIL4r, yielding the first solution box $[\boldsymbol{u}_t^{\diamond}]^{(1)}$. In other words, PIL4r is a simplified version of PIL4 not performing the contraction phase that iterates the combined constraints in the forward-backward contractor. The anchors are first assumed to be randomly deployed with a density of 0.015 anchor per m^2. The distribution of anchors is generated 5 times and all results are averaged over the 5 cases. TABLE VI shows the average boxes areas, the average estimation errors and the average computation costs per time-step obtained with PIL4 and PIL4r. The use of the contraction phase in PIL4 leads thus to a slightly higher accuracy, at the cost of a high increase of the computation time. 100 uniformly deployed anchors are then considered. The results of both methods are illustrated in TABLE VII. As expected, PIL4 yields at least as much accuracy as PIL4r, with higher computation times due to the iteration of more constraints. In the following, the relaxed version PIL4r of the method is considered, since it leads to almost the same accuracy as PIL4 with less computation time.

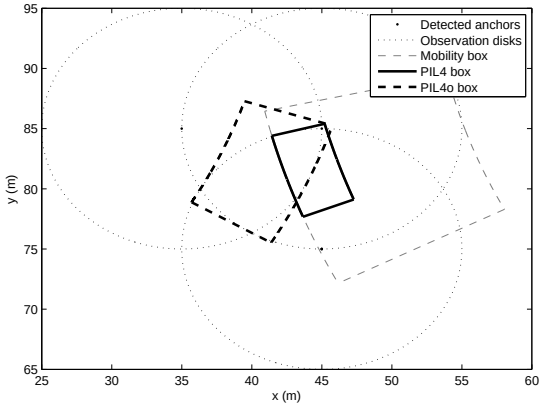

Fig. 11. Estimated boxes obtained with PIL4 and PIL4o at time-step 70.

TABLE VI
COMPARISON OF PIL4 TO PIL4R WITH RANDOMLY DEPLOYED ANCHORS.

Methods	Boxes areas	Estimation errors	Computation times
PIL4	$64.44m^2$	$1.99m$	$0.0064s$
PIL4r	$66.08m^2$	$2.11m$	$0.00088s$

TABLE VII
COMPARISON OF PIL4 TO PIL4R WITH UNIFORMLY DEPLOYED ANCHORS.

Methods	Boxes areas	Estimation errors	Computation times
PIL4	$59.77m^2$	$2.01m$	$0.0037s$
PIL4r	$60.17m^2$	$2.02m$	$0.00055s$

D. Impact of the anchors density

This section studies the impact of the anchors density on the estimation results of the proposed method PIL4r. The number of anchors is varied from 25 to 225 and the distribution of anchors is assumed to be uniform. With the increase of the anchors density in the network, the average number of detected anchors per time step varies from 0.78 to 7.1. In other words, the number of constraints to be considered in the algorithm is increased, leading to an increase of the estimation accuracy as well as an increase of the computation time. Fig. 12 illustrates the average number of detected anchors, the estimation error, the boxes areas and the computation time as a function of the number of anchors uniformly deployed in the network. As expected, the more we have anchors in the network, the more estimation is accurate and the more the computation time increases.

E. Comparison to another interval-based method

In this section, the proposed method is compared to an interval-based method using cartesian coordinates, as shown in [8]. Using both observation and mobility models, this method, denoted by CIL, yields rectangular boxes estimates covering all possible solutions. 100 uniformly deployed anchors are first considered. Fig. 13 shows the boxes obtained using the PIL4r and the CIL methods, whereas TABLE VIII illustrates the computation results. It is obvious that with a uniformly deployed distribution of anchors, PIL4r yields much higher accuracy than CIL. 150 anchors are then randomly deployed

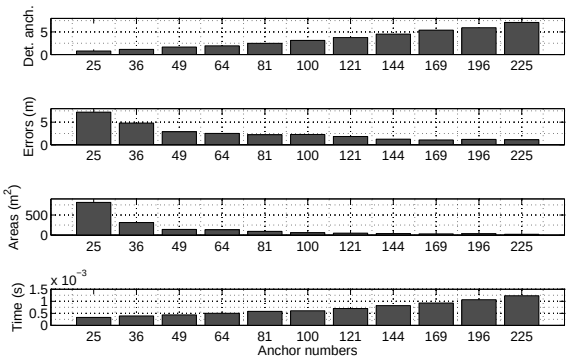

Fig. 12. Impact of the anchors density.

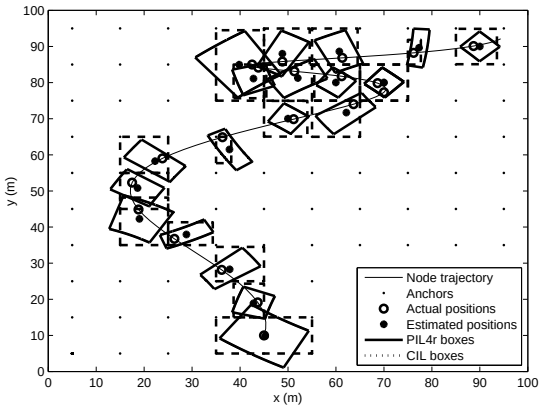

Fig. 13. Estimated boxes obtained with PIL4r and CIL.

over the surveillance area, in 5 different manners. TABLE IX shows the computation results averaged over the 5 cases. As shown in the results table, PIL4r still provide more accurate estimation but here the difference between both results is minor. Indeed, the accuracy of both methods is tightly related to the shape of the solution area, which depends on the distribution of the anchors in the network.

F. Comparison to a Monte-Carlo-based method

This section compares the proposed method to a Monte-Carlo-based method [7]. This method, called MCL, yields at each time step a fixed number N of positions, called particles, in the way to best cover the solution area. The estimated positions using MCL correspond to the centers of the computed particles. N is first set to 50. Fig. 14 shows the estimated particles using MCL as well as the estimated boxes using PIL4r with 100 uniformly deployed anchors. Let the estimation errors of MCL be the distances between the centers of the particles and the actual positions. TABLE X shows the average estimation errors and the average computation times per time-step obtained with PIL4r and MCL while using 50 and 20 particles. According to these results, the MCL method leads at some time-steps to particles covering precisely the solution area but it remains less accurate than PILr4 with more computation time even with less particles. It is also more consuming in terms of memory resources. One could reduce

TABLE VIII
COMPARISON OF PIL4R TO CIL WITH UNIFORMLY DEPLOYED ANCHORS.

Methods	Boxes areas	Estimation errors	Computation times
PIL4r	$60.17m^2$	$2.02m$	$0.00055s$
CIL	$88.80m^2$	$3.01m$	$0.0016s$

TABLE IX
COMPARISON OF PIL4R TO CIL WITH RANDOMLY DEPLOYED ANCHORS.

Methods	Boxes areas	Estimation errors	Computation times
PIL4r	$66.08m^2$	$2.11m$	$0.00088s$
CIL	$66.64m^2$	$2.37m$	$0.0028s$

the memory and the computation time consumptions by using less particles, however with less particles, the solution area would not be well covered. TABLE XI shows the computation results obtained with 150 randomly deployed anchors averaged over 5 distributions. Here also PIL4r leads to more accurate estimates with less computation time.

V. CONCLUSION

This paper proposes an original technique for sensors localization in wireless sensor networks. The proposed approach is an anchor-based method using connectivity measurements, as well as the mobility of the nodes. Based on interval analysis, the solution is provided using polar intervals. An outer approximation of the solution is thus performed in four different polar coordinate systems. Instead of exact estimates, the proposed method yields partial rings including for sure all the possible solutions of the problem. Simulation results corroborate the efficiency of the proposed method compared to other methods based on Monte-Carlo or cartesian intervals. Future works will consider the problem under imperfect circumstances, where a robust extension of the proposed method would be proposed. Realistic simulations based on real sensors with real RSSI measurements would also be considered.

REFERENCES

[1] I. F. Akyildiz, W. Su, Y. Sankarasubramaniam, and E. Cayirci, "A survey on sensor networks," *IEEE Communications Magazine*, vol. 40, pp. 102–114, 2002.
[2] R. Shorey, Ed., *Mobile, Wireless, and Sensor Networks: Technology, Applications, and Future Directions*. John Wiley & Sons, 2006.
[3] http://www.mobilerobots.com/ResearchRobots/ResearchRobots.aspx.
[4] K. Dantu, M. Rahimi, H. Shah, S. Babel, A. Dhariwal, and G. S. Sukhatme, "Robomote: Enabling mobility in sensor networks," in *IEEE/ACM Fourth International Conference on Information Processing in Sensor Networks (IPSN-SPOTS)*, 2005, pp. 404–409.
[5] Y. Zou and K. Chakrabarty, "Distributed mobility management for target tracking in mobile sensor networks," *IEEE Transactions on Mobile Computing*, vol. 6, no. 8, pp. 872–887, August 2007.
[6] F. Mourad, H. Chehade, H. Snoussi, F. Yalaoui, L. Amodeo, and C. Richard, "Controlled mobility sensor networks for target tracking using ant colony optimization," *IEEE Transactions on Mobile Computing*, vol. 11, no. 8, pp. 1261–1273, 2011.
[7] L. Hu and D. Evans, "Localization for mobile sensor networks," in *Tenth annual international conference on mobile computing and networking (MobiCom)*, Philadelphia, USA, 2004.
[8] F. Mourad, H. Snoussi, F. Abdallah, and C. Richard, "Anchor-based localization via interval analysis for mobile ad-hoc sensor networks," *IEEE Transactions on Signal Processing*, vol. 57, no. 8, pp. 3226–3239, 2009.

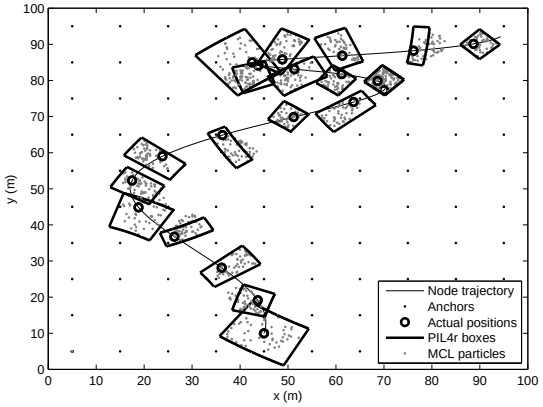

Fig. 14. Estimated boxes with PIL4r and particles obtained using MCL.

TABLE X
COMPARISON OF PIL4R TO MCL WITH UNIFORMLY DEPLOYED ANCHORS.

Methods	Estimation errors	Computation times
PIL4r	$2.02m$	$0.00055s$
MCL ($N = 50$)	$2.77m$	$0.021s$
MCL ($N = 20$)	$2.87m$	$0.019s$

TABLE XI
COMPARISON OF PIL4R TO MCL WITH RANDOMLY DEPLOYED ANCHORS.

Methods	Estimation errors	Computation times
PIL4r	$2.11m$	$0.00088s$
MCL ($N = 50$)	$2.65m$	$0.034s$
MCL ($N = 20$)	$2.67m$	$0.031s$

[9] G. Song, Y. Zhou, F. Ding, and A. Song, "A mobile sensor network system for monitoring of unfriendly environments," *Sensors*, vol. 8, pp. 7259–7274, November 2008.

[10] R. Tharmarasa, T. Kirubarajan, A. Sinha, and T. Lang, "Decentralized sensor selection for large-scale multisensor-multitarget tracking," *IEEE Transactions on Aerospace and Electronic Systems*, vol. 47, no. 2, pp. 1307–1324, 2011.

[11] G. Zanca, F. Zorzi, A. Zanella, and M. Zorzi, "Experimental comparison of RSSI-based localization algorithms for indoor wireless sensor networks," in *REALWSN*, Glasgow, United Kingdom, April 2008.

[12] R. Li, Z. Fang, B. Hao, and F. Yang, "Research on indoor wireless localization system for radioactive sources based on zigbee," in *International Conference on Computing, Control and Industrial Engineering (CCIE)*, vol. 2, june 2010, pp. 359–362.

[13] B. Hofmann-Wellenhof, H. Lichtenegger, and J. Collins, *Global Positioning System: Theory and Practice*. Springer, September 2004.

[14] J. Shen and A. Molisch, "Passive location estimation using TOA measurements," in *IEEE International Conference on Ultra-Wideband (ICUWB)*, sept. 2011, pp. 253–257.

[15] R. Eickhoff, F. Ellinger, R. Mosshammer, R. Weigel, A. Ziroff, and M. Huemer, "3D-accuracy improvements for TDoA based wireless local positioning systems," in *IEEE GLOBECOM Workshops*, nov. 30-dec. 4 2008, pp. 1–6.

[16] J. Tai, S. Y. Tan, and C. K. Seow, "Three-dimensional non-line-of-sight localisation in an indoor multipath environment," in *7th International Conference on Information, Communications and Signal Processing (ICICS)*, dec. 2009, pp. 1–5.

[17] D. Niculescu and B. Nath, "Dv based positioning in ad hoc networks," *Telecommunication Systems*, vol. 22, no. 1-4, pp. 267–280, 2003.

[18] J. Yi, S. Yang, and H. Cha, "Multi-hop-based monte carlo localization for mobile sensor networks," San Diego, CA, USA, 2007.

[19] D. Bertsimas, D. Brown, and C. Caramanis, "Theory and applications of Robust Optimization," *SIAM Review*, vol. 53, no. 3, pp. 464–501, 2011.

[20] J. Teng, H. Snoussi, and C. Richard, "Decentralized variational filtering for simultaneous sensor localization and target tracking in binary sensor networks," in *IEEE International Conference on Acoustics, Speech and Signal Processing (ICASSP)*, april 2009, pp. 2233–2236.

[21] F. Mourad, H. Snoussi, and C. Richard, "Interval-based localization usinf RSSI comparision in MANETs," *IEEE Transactions on Aerospace and Electronic Systems*, vol. 47, no. 4, pp. 2897–2910, 2011.

[22] A. Paul and E. Wan, "RSSI-based indoor localization and tracking using Sigma-Point Kalman Smoothers," *IEEE Journal of Selected Topics in Signal Processing*, vol. 3, no. 5, pp. 860–873, oct. 2009.

[23] L. Jaulin, M. Kieffer, O. Didrit, and E. Walter, *Applied interval analysis*. Springer, 2001.

[24] A. Medeisis and A. Kajackas, "On the use of the universal okumura-hata propagation prediction model in rural areas," in *Vehicular Technology Conference Proceedings*, vol. 3, VTC Tokyo, May 2000, pp. 1815–1818.

Farah Mourad was born in January 15, 1984. She received the diploma degree in electrical engineering from the Lebanese University, Faculty of Engineering, Tripoli, Lebanon, in 2006. She also received the Master degree, in 2007, and the Ph.D., in 2010, in systems optimization and security from the University of Technology of Troyes, France (UTT). Since September 2011, she has been an associate professor at the UTT. Her research interests include wireless and mobile sensor networks, nonlinear signal analysis, machine learning and biomedical applications.

Paul Honeine (M'07) received the Dipl.-Ing. degree in 2002 and the M.Sc. degree in 2003, both from the Faculty of Engineering, the Lebanese University, Lebanon. In 2007, he received the Ph.D. degree in systems optimization and security from the University of Technology of Troyes, France (UTT), and was a Postdoctoral Research associate with the Systems Modeling and Dependability Laboratory, from 2007 to 2008. Since September 2008, he has been an assistant Professor at the UTT. His research interests include nonstationary signal analysis, nonlinear signal processing, sparse representations, machine learning, and wireless sensor networks. He is the co-author (with C. Richard) of the 2009 Best Paper Award at the IEEE MLSP Workshop.

Hichem Snoussi was born in Bizerte, Tunisia, in 1976. He received the diploma degree in electrical engineering from the Ecole Suprieure d'Electricit (Supelec), Gif-sur-Yvette, France, in 2000. He also received the DEA degree and the Ph.D. in signal processing from the University of Paris-Sud, Orsay, France, in 2000 and 2003 respectively. He has obtained the HdR from the University of Technology of Compigne in 2009. Between 2003 and 2004, he was postdoctoral researcher at IRCCyN, Institut de Recherches en Communications et Cyberntiques de Nantes. He has spent short periods as visiting scientist at the Brain Science Institute, RIKEN, Japan and Olin Neuropsychiatry Research Center at the Institute of Living in USA. Between 2005 and 2010, he has been associate professor at the University of Technology of Troyes. Since September 2010, he has been appointed a Full Professor position at the same university. He is in charge of the regional research program S3 (System Security and Safety) of the CPER 2007-2013 and the CapSec plateform (wireless embedded sensors for security). He is the principal investigator of an ANR-Blanc project (mv-EMD), a CRCA project (new partnership and new technologies) and a GDR-ISIS young researcher project. He is partner of many ANR projects, GIS, strategic UTT programs. He obtained the national doctoral and research supervising award PEDR 2008-2012.